A Theoretical Study of Hydrolysis by Phospholipase A_2: The Catalytic Role of the Active Site and Substrate Specificity

Bohdan Waszkowycz and Ian H. Hillier*
Department of Chemistry, University of Manchester, Manchester M13 9PL
Nigel Gensmantel and David W. Payling
Fisons plc, Pharmaceuticals Division, Bakewell Road, Loughborough, Leicestershire LE11 0RH

A computational model, which involves the combination of molecular mechanics and molecular-orbital methods, has been developed to study the energetics of phospholipid hydrolysis in the active site of phospholipase A_2. This model has been found to explain the catalytic role of the active site and is able to quantify differences in binding and hydrolysis between an ester and amide substrate. The mechanism of catalysis proposed on the basis of structural data is shown to be in accord with currently available experimental data.

The enzyme phospholipase A_2 (PLA2) plays a fundamental role in cell regulation, being responsible for the hydrolysis of the phospholipids of cell membranes to release fatty acids such as arachidonic acid, and thereby initiating the production of a diverse range of cellular mediators such as the prostaglandins.[1] Inhibition of PLA2 is a potentially important route to the treatment of various inflammatory disorders, and therefore an understanding of the mechanism of catalysis may contribute to rational drug design.

A mechanism has been proposed by Verheij *et al.*[2] based on the X-ray crystal structure of PLA2, which shows similarities to other hydrolytic enzymes, in particular the serine proteases. As there has been insufficient experimental evidence to date to prove this mechanism, the application of theoretical calculations offers a potentially powerful method with which to explore in detail aspects of catalysis which may not be readily determined by experiment.

In an earlier paper[3] we presented preliminary calculations on the energetics of phospholipid hydrolysis by PLA2, by means of *ab initio* molecular orbital calculations on a simple model of the substrate and important active-site residues, which provided evidence in favour of the Verheij mechanism. In this paper, we describe extensions of these calculations to present a more thorough description of the binding and hydrolysis of a phospholipid substrate and an amide inhibitor, and to account for the substrate specificity of PLA2.

In recent years, the combination of quantum chemical and empirical force-field methods has proved to be a powerful technique for the study of enzyme catalysis. Molecular mechanics (MM) can readily be applied to macromolecular systems to explore the structure and the conformational or binding energies of enzyme–substrate/inhibitor complexes.[4,5] However, molecular orbital (MO) methods are necessary to evaluate the energetics of bond formation or breaking, but are restricted, by computational expense, to modelling only a small region of the active site.

The quantum mechanical model can be extended if the bulk of the enzyme is represented by a field of point charges incorporated into the one-electron Hamiltonian. By this method, it is possible to simulate the electrostatic influence of the macromolecular environment on the electronic wavefunction of the quantum mechanical (QM) system, and thus to model the activation of a substrate or the stabilisation of a transition state, as demonstrated by work on carboxypeptidase,[6–8] papain,[9] and trypsin.[10,11]

A complete description of the system is achieved by the combination of the above methods, in which MM is used to determine the geometric structure of the enzyme–substrate complex (and to evaluate conformational energy), while reserving an MO method to evaluate the electronic energy of fragments of active site residues involved in catalysis. The potential energy surface for the reaction is thus described in terms of both QM and MM energies. Such an approach has been applied to the investigation of catalysis in papain,[12] triosephosphate isomerase,[13] and trypsin.[14]

More recently, the more formal integration of MO and MM methods has been developed in order to build combined QM–MM models in which MM forces exerted by the bulk environment are allowed to influence the geometry optimisation of the QM system.[15,16] Thus a reactive intermediate can be modelled *in situ* rather than *in vacuo*, with the steric and electrostatic interactions of the QM system with the MM environment taken into account.

In the work described herein, we have used MM as implemented in the program AMBER[17] and computer graphics to model the complexes formed between PLA2 and a phospholipid substrate, an amide inhibitor, and the oxyanions assumed to be intermediates in their hydrolysis, for which no X-ray structures are available. From these MM structures, we built models of the active site, which are used in the MO program GAMESS,[18] to evaluate the energetics of substrate hydrolysis both *in vacuo* and *in situ*. The latter includes the incorporation into the Hamiltonian of point charges representing a substantial amount of the enzyme. The structure of the QM system of this hybrid QM–MM model is first refined by means of QM optimisations which employ combined QM–MM gradients, and follow the methodology suggested by Singh and Kollman.[16]

The relative free energies of binding of the substrate and inhibitor are estimated by the free-energy perturbation method,[19,20] as implemented in the GIBBS module of AMBER.[21] Here, a statistical mechanics approach is taken to evaluate the Gibbs free-energy change for a perturbation to a system. The use of molecular dynamics allows the evaluation of ensemble averages of interaction energies, which avoids the errors in the determination of enthalpies that are inherent in the MM method because of the neglect of sampling of conformational space. The free-energy perturbation method has proved useful in evaluating free energies of substrate binding[22–24] and the effects on catalysis of amino acid mutation,[25,26] which are consistent with experimental values.

The proposed mechanism of PLA2 catalysis can be described briefly.[2] PLA2 hydrolyses only the 2-acyl ester bond of 1,2-

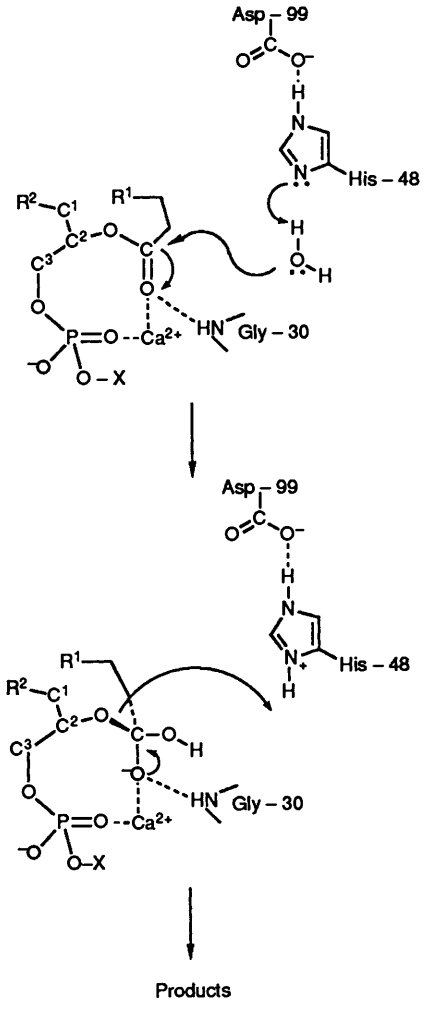

Figure 1. Proposed mechanism of catalysis in PLA2.

diacyl-*sn*-3-glycerophosphatides (L-α-phospholipids). A histidine ring (His-48 of bovine pancreatic PLA2) and a calcium ion are known to be essential for activity. His-48 is buried within the hydrophobic wall of the active site cleft, hydrogen bonded to an aspartate carboxylate (Asp-99), a feature similar to the serine–histidine–aspartate triad of the serine proteases. In PLA2, a water molecule is proposed to be the active nucleophile in the absence of serine or cysteine. The phospholipid substrate is said to bind to the calcium ion *via* the C^2 carbonyl and a phosphoryl oxygen, with the acyl chains interacting with the hydrophobic wall (Figure 1). The polarised carbonyl is attacked by a water molecule (present in the crystal structure), with proton transfer to His-48, which leads to the formation of a tetrahedral oxyanion intermediate, stabilised by the calcium ion and a hydrogen bond to Gly-30. Proton transfer from His-48 to the C^2 ether oxygen results in the breakdown of the intermediate and the release of the C^2 fatty acid. In the original description of the serine protease charge relay triad, it was suggested that a second proton transfer occurs between the protonated histidine and aspartate, so that the ionic couple becomes neutral.[27] In the original mechanism for PLA2, this second proton transfer was also assumed to take place. However, recent experimental[28,29] and computational[10,11,30] work has shown that this double proton transfer does not occur in the serine proteases, and therefore we take the opportunity here to determine whether it is likely to be found in PLA2.

Our earlier calculations[3] demonstrated that this mechanism

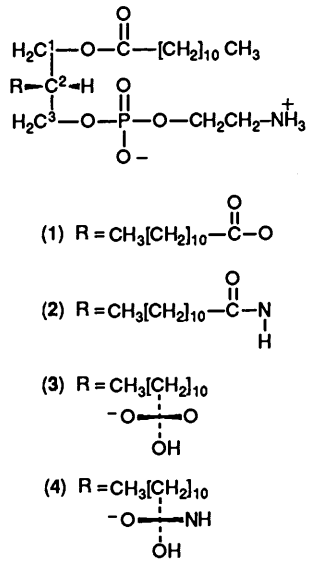

is feasible and that the calcium plays a major role in the stabilisation of the oxyanion. Here we develop a computational model which is a better representation of the enzyme, and which can provide further insight into the mechanisms of catalysis and substrate specificity.

Computational Details.—MM Modelling. Models of PLA2 substrate complexes were built in AMBER with the aid of computer graphics, based on the crystal structure of bovine pancreatic PLA2.[31] The substrates considered were a phospholipid, 1,2-dilauryl-3-*sn*-phosphatidylethanolamine (**1**), an amide analogue (**2**) known to be a competitive inhibitor, and the oxyanions (**3**) and (**4**) presumed to be intermediates in their hydrolysis. These we assume to approximate the true transition states in structure and energy, and therefore we can use the difference in the QM energy between the substrate and the oxyanion as a measure of the true potential-energy barrier.

The complete enzyme (123 amino acid residues) was treated in the MM calculations. To the 106 water molecules in the X-ray structure were added a further 640 water molecules in order to produce a complete solvation shell around the enzyme. This solvated PLA2–substrate model consisted of approximately 3 500 atoms. The united atom representation[32] was used for the bulk of the system with the all-atom force-field[33] for the 16 residues within the active site and for the substrates. (In AMBER the calcium ion is treated only by van der Waals and electrostatic terms). In those cases where force-field parameters were unavailable (*e.g.* for the oxyanion), suitable parameters were taken from STO-3G optimisations of model compounds. (At this stage, approximate parameters are sufficient as these geometries are to be refined using the combined QM–MM method at a later stage). Partial charges were determined by the electrostatic potential method of Singh and Kollman[34] using an STO-3G basis set. The conformation of the substrates was based on the X-ray structure of the phospholipid (**1**).[35] The phospholipid was initially positioned in the active site in accordance with the Verheij mechanism, with the C^2 carbonyl bound to the calcium ion and the acyl chains extended from the active site into the solvent. This conformation was retained after MM minimisation of the complete system. The amide analogue was minimised in the active site in the same manner. All minimisations employed a dielectric of 1 and a non-bonded cut-off of 8 Å. Conjugate gradient minimisation was performed to a root-mean-square gradient of at least 0.1 kcal $Å^{-1}$.

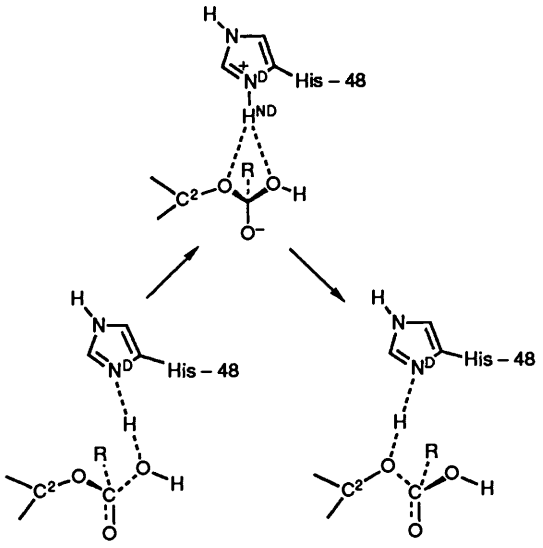

Figure 2. Proposed mechanism of formation and breakdown of the oxyanion tetrahedral intermediate.

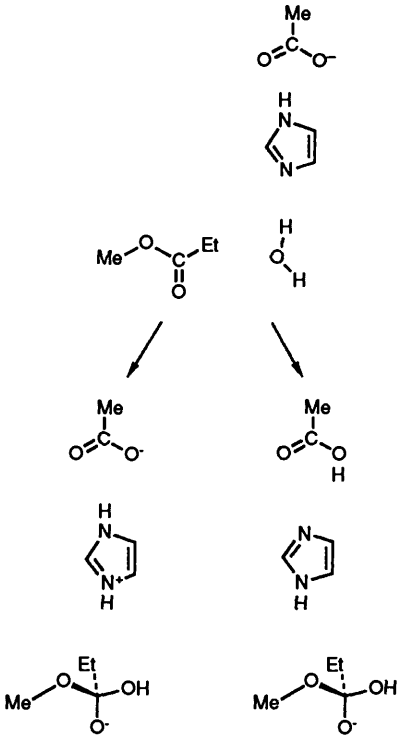

Figure 3. Molecules considered explicitly in the MO calculations. (Methyl propanoate models the ester phospholipid; similarly, *N*-methyl propanamide models the amide phospholipid). The two reaction paths depict the single and double proton transfer mechanisms, respectively.

Initial minimisations of the oxyanions resulted in the adoption of a position very similar to the substrates, where the hydroxy oxygen is hydrogen bonded to H^{ND} of the protonated His-48 but with the C^2 alkoxy oxygen some 3–4 Å away from H^{ND}. In the proposed mechanism, H^{ND} (the proton transferred to His-48 from the attacking water) must be transferred to the C^2 alkoxy oxygen on breakdown of the oxyanion. For this to happen readily, H^{ND} must be within hydrogen-bonding distance of the alkoxy oxygen. Trial minimisation showed that oxyanions formed from small esters fit readily into the active site to form the doubly hydrogen-bonded structure (Figure 2), which suggests that the phospholipid oxyanion is prevented from doing so by a local conformational energy barrier. Therefore the phospholipid oxyanion was minimised by use of constraints to force the desired hydrogen bonds, and then allowed to relax into the first local potential energy minimum. Such a doubly hydrogen-bonded structure is similar to that proposed to form during the hydrolysis of the acyl intermediate in the serine proteases.[28,29]

QM–MM Calculations. The structures of the PLA2–substrate complexes modelled above were simplified for the combined QM–MM calculations. An active-site model was built which comprised those residues within about 15 Å of the centre of the active site (68 amino acid residues, 50 water molecules) to give a system of about 1 000 atoms. The QM atoms of the system were taken to be the side chains of His-48 and Asp-99, the attacking water and a portion of the substrate surrounding the C^2 carbonyl (Figure 3). The geometries of the QM residues were first refined, so as to be consistent with an STO-3G basis set. For the substrate/oxyanion head-group this was achieved by a QM optimisation *in situ*, by incorporation of the MM gradients (exerted by the MM atoms on the QM atoms) into the QM optimisation of the QM atoms. Hence the QM optimisation is influenced by MM gradients across the MM–QM junction (bond, angle, and dihedral forces) and between non-bonded pairs (van der Waals, hydrogen bond and, if required, electrostatic forces). Therefore, this is a potentially useful method to model accurately the *in situ* structures of species such as the oxyanion, rather than to rely on the MM minimised geometry.

Our use of the STO-3G basis set is not ideal, but was chosen in view of the size of the molecules involved and the large number of steps required to achieve convergence of the optimisations. (Single-point calculations were performed at higher basis sets to obtain QM energies). During the optimisation, the remainder of the substrate, as well as the active site, was held fixed. The partial charges of all atoms in the environment were incorporated into the Hamiltonian, which was found to be more effective than treatment of the electrostatic interaction between QM and MM systems with a MM electrostatic gradient. We found that in this system, electrostatic gradients are very large and prevent optimisation of the QM atoms. The hybrid QM–MM method was modified so that all QM atoms experienced the same field of point charges, with the omission of charges of carbon atoms at QM–MM junctions which are replaced by hydrogens to fill out the valency of the QM systems. Although some point charges may be close to the QM atoms, no problems were observed due to inappropriate polarisation of the wavefunction.

The QM system depicted in Figure 3 may appear somewhat large, but this is necessary in order to allow the QM atoms a realistic degree of conformational freedom during optimisation, when the QM system is anchored in space at each QM–MM junction. A further advantage of having a large QM system is that it avoids spuriously large MM gradients when, for example, the ester sp^2 carbon rehybridizes to sp^3. Thus, all distortions of geometry are contained within the QM system.

After optimisation of the substrate headgroup by the hybrid QM–MM method, the active site was refined by a further MM minimisation in which the geometries of the side-chains of His-48 and Asp-99 and the attacking water were constrained to their STO-3G *in vacuo* geometries. The remainder of the active site was held fixed during this minimisation apart from those groups directly hydrogen-bonded to His-48 and Asp-99 (two tyrosine hydroxy groups and several water molecules) and part of the substrate alkyl chains immediately adjacent to the QM system (in order to relieve any large gradients which arise across the QM–MM junction).

The result of this series of minimisations is to produce models of the substrates/oxyanions in the active site, in which all the

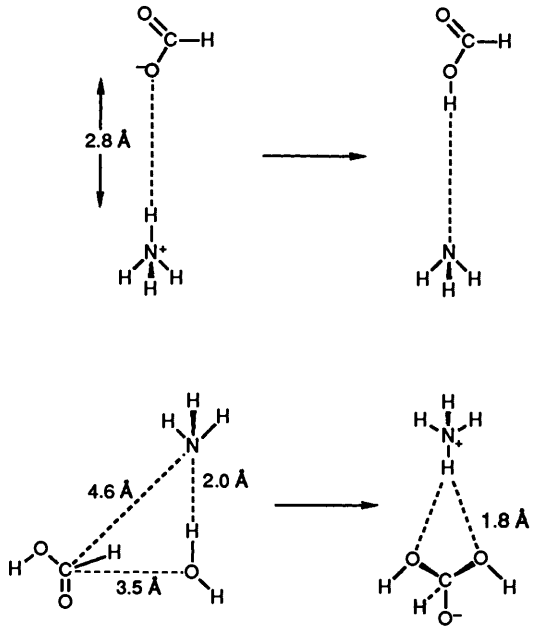

Figure 4. Supermolecule models used for the large basis set MO calculations. Formamide replaces formic acid in the amide model. A single point charge of +1 (model VIb) was positioned at 3 Å from the carbonyl oxygen, at an angle of 180° to the carbonyl.

intramolecular geometries of all QM residues are consistent with the STO-3G basis set, while all intermolecular geometries are determined by MM. The final models are then used to perform single-point MO calculations as described below.

In each system, the difference in quantum-mechanical energy (ΔE_{QM}) between the substrate model and the respective oxyanion model is used as a measure of the barrier to ester hydrolysis for the particular reaction. Reactions described as *in vacuo* treat all atoms explicitly in the QM calculation, while those described as *in situ* incorporate the partial charges of all atoms of the active site model into the Hamiltonian (approximately 1 000 atoms in total). Charges were omitted for methylene groups at QM–MM junctions, as were any very small charges (<0.01 e). All charges were standard AMBER peptide charges. For both the ester and amide substrates, the following reactions were considered.

Model I: ester + imidazole + water ⟶
oxyanion + imidazolium

Model IIa: ester + imidazole + water + acetate ⟶
oxyanion + imidazolium + acetate

Model IIb: as for IIa but treated *in situ*

For the ester substrate the following models of the double proton transfer were also evaluated.

Model IIIa: ester + imidazole + water + acetate ⟶
oxyanion + imidazole + acetic acid

Model IIb: as for IIIa but treated *in situ*

(The models for the double proton transfer assume a dihedral angle of 180° for Asp-99 O^{D1}–C^{G}–O^{D2}–H.)

The single-point evaluations of ΔE_{QM} employed a 4-31G basis set as a compromise between the need to use as large a basis set as possible, and the need to include explicitly a large proportion of the active site. STO-3G is known to be a poor basis set for the reproduction of relevant proton affinities, while 4-31G has been shown to give results consistent with experimental data[30] and has been widely used for systems of this nature.[7] However, as described later, we have estimated the accuracy of 4-31G by performing some representative calculations using larger basis sets (up to 6-31G**/MP2).

In a further series of single-point calculations, small modifications were made to the field of point charges to investigate the dependence of ΔE_{QM} on the immediate environmental of the QM atoms, in particular by modification of the charge which represents the calcium ion.

For the above models, the MM energy of interaction between the QM and MM systems was calculated by use of MM, in terms of bond/angle/dihedral energies across the QM–MM junction, and van der Waals and hydrogen-bond energies between non-bonded atoms (but with no electrostatic terms). This provides a measure of the stabilisation of the substrate/oxyanion by the active site, other than by the purely electrostatic contribution included in the *in situ* QM calculation.

Large Basis Set QM Calculations. A series of test cases were evaluated in order to determine the basis set dependency of the QM calculations. The QM system was considerably reduced (Figure 4). Thus the ester/amide substrates were modelled by formic acid/formamide respectively, His-48 by ammonia and Asp-99 by formate. Supermolecule models were built with *in vacuo* STO-3G geometries for each species and intermolecular geometries which approximated those in PLA2. The calcium ion was simulated in certain models as a simple +1 point charge, 3 Å from the carbonyl oxygen. These models were not intended to be directly comparable to the previous active site models, but merely to demonstrate the sensitivity of ΔE_{QM} on the choice of basis set. The basis sets used were STO-3G, 4-31G, 6-31G**, and 6-31G**/MP2, the latter including electron correlation at the level of second-order Moller–Plesset perturbation theory as implemented in the program CADPAC.[36]

Free-energy Perturbation Calculations. The free energy perturbation method was used to determine the relative free energies of desolvation and binding of the ester and amide phospholipids, based on the following thermodynamic cycle:[19]

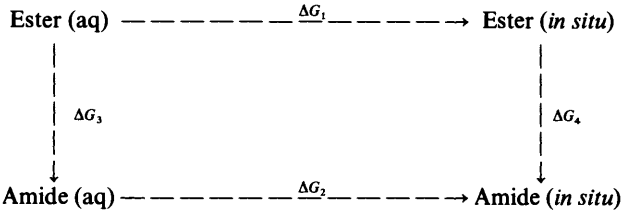

Although the relative free-energy of binding ($\Delta\Delta G_B$) between ester and amide is $\Delta G_2 - \Delta G_1$, the evaluation of these free energies involves the simulation of substrate desolvation followed by binding to the active site. Both these processes involve large-scale disruption to the macromolecular system and hence are difficult to simulate accurately. The non-physical process of mutation of the ester into the amide causes minimal disruption to the system and hence can be simulated with higher accuracy, to provide $\Delta\Delta G_B = \Delta G_4 - \Delta G_3$. (In the case of PLA2 the evaluation of desolvation energies may not be wholly appropriate in as much as the substrates are initially bound in the lipid membrane and are not free monomers in aqueous solution. However, the calculation serves as a check on the methodology).

Desolvation free energies were determined for small model substrates (methyl acetate and *N*-methylacetamide) in a box of approximately 260 water molecules, by use of partial charges

calculated by the electrostatic potential method with an STO-3G basis set. The system was first equilibrated with 4 ps of molecular dynamics (2 000 × 2 fs steps) at constant temperature (300 K) and pressure (1 atm), by use of periodic boundary conditions (8 Å non-bonded cut-off). The SHAKE algorithm was employed to freeze bond lengths during all molecular dynamics. For the free energy perturbation calculation, the 'window' technique was used, in which the mutation of amide to ester was accomplished in a series of 21 discrete steps, during which the (classical) Hamiltonian was incremented at each step. Each window comprised 500 × 2 fs steps of molecular dynamics to equilibrate the system followed by 500 × 1 fs steps for data collection. Forward and reverse energies are calculated at each window to give ΔG for the overall mutation in both directions. The calculation was repeated in the reverse direction (ester to amide) in order to test the dependency of the results on the starting conformation of the system. Therefore ΔG is expressed as the mean of the 4 values obtained. The standard deviation quoted refers to the statistical reproducibility of the method and does not reflect error in the force-field or choice of partial charges.

Binding free energies were calculated for the full phospholipid ester and amide within PLA2. The model comprised the whole enzyme as before, but with the shell of water replaced by a spherical cap of water molecules of radius 15 Å from the C^2 carbonyl. To these 120 were added 5 water molecules (from the previous MM model) found hydrogen-bonded within the active site. During the simulations, residues further than approximately 12 Å from the carbonyl were held fixed so that some 46 residues, plus the calcium and all the substrate and water, were allowed to be mobile. This partial freezing of the enzyme is necessary if the entire enzyme is not to be fully solvated, and also prevents gross distortions of the enzyme during prolonged simulation. During simulation, the water molecules are prevented from evaporating by means of a harmonic potential of 0.5 kcal mol^{-1}. Partial charges for the C^2 carbonyl headgroup were determined by the hybrid QM–MM method with the inclusion of the partial charges of the active site in the Hamiltonian. This allowed the calculated charges to be polarised by the active site, to reflect the considerable polarisation of the carbonyl group by the calcium ion.

Following an initial MM minimisation to tidy the added waters, the system was equilibrated (1 000 × 0.5 fs steps, followed by 1 000 × 1 fs steps and 2 000 × 2 fs steps, to give 5.5 ps in total), at constant temperature (but without periodic boundary conditions). The free energy perturbation calculation was performed both by the window method (again 21 windows of 500 × 2 fs equilibration and 500 × 1 fs data collection) and also by the 'slow growth' method (perturbation of the classical Hamiltonian over each of 20 000 × 1 fs steps).

The QM, MM, and molecular dynamics calculations were performed on the FPS M64/60 of the Computational Chemistry Group of Manchester University, and on the CRAY XMP/28 of the University of London Computer Center.

Results and Discussion

It has been demonstrated experimentally that amide analogues similar to (2) bind to PLA2 more strongly than the respective esters (with a 5–10 fold difference in binding constants) but are not hydrolysed.[37,38] Experimental data for the interaction of PLA2 with trial substrates tend to be semi-quantitative because of limitations in the assay technique, which arise from the requirement that the substrate must be aggregated (micellar) in order to obtain a measurable rate of catalysis. Hence inhibitors must also be incorporated into micelles, which leads to problems when the critical micelle concentration of substrate and inhibitor are dissimilar, or when the affinities of PLA2 for the mixed micelle and for pure substrate are dissimilar.[38] Therefore, such physical effects cause difficulties in the interpretation of biochemical data in terms of rates of catalysis and binding affinities.

However, for our purposes we are satisfied with devising a computational model which will describe semi-quantitatively the mechanism of catalysis and substrate selectivity of PLA2, while recognising that many approximations remain in our computational method.

MM Calculations.—The structures of the MM minimised PLA2–substrate complexes can only be confirmed when X-ray crystal structures have been obtained. However, our models are consistent, as far as possible, with the experimental data available and with the Verheij mechanism, and are qualitatively similar to MM models developed by other workers.[39] There is the possibility that PLA2 may undergo major conformational change on interaction with the lipid membrane, which we cannot simulate. However, our results give no reason to suggest that the crystal structure is not appropriate for discussion of the enzyme–substrate interactions.

The MM minimisations revealed that no significant conformational change to the enzyme is required in order to fit a phospholipid into the active site, with minimal deformation of the flexible phospholipid from its 'tuning-fork' crystal conformation (mostly at the C^3 chain). The mean displacement of the peptide backbone atoms between the original PLA2 crystal structure and the minimised PLA2–substrate complex was 0.53 ± 0.24 Å. Table 1 presents key interatomic distances to

Table 1. Examples of interatomic distances (in Å) within the active site of PLA2, and comparison of the X-ray structure with MM-minimised models, as follows: A, X-ray PLA2 co-ordinates; B, minimised PLA2-ester phospholipid; C, minimised PLA2-ester oxyanion phospholipid; D, minimised PLA2-amide phospholipid; E, minimised PLA2-amide oxyanion phospholipid.

	A	B	C	D	E
Environment of calcium loop					
CAL^b–O(Tyr-28)	2.28	2.29	2.29	2.29	2.29
CAL–O(Gly-30)	2.47	2.33	2.36	2.34	2.35
CAL–O(Gly-32)	2.32	2.34	2.53	2.38	2.45
CAL–O^{D1}(Asp-49)	2.66	2.28	2.27	2.28	2.26
CAL–O^{D2}(Asp-49)	2.47	2.29	2.44	2.30	2.39
Environment of His–Asp couple					
N^D(His-48)–O(Wat-1)	3.09	2.91	—	2.99	—
N^E(His-48)–O^{D2}(Asp-99)	2.78	2.71	2.59	2.70	2.59
O^{D2}(Asp-99)–O^H(Tyr-52)	2.55	2.87	2.80	2.61	2.89
O^{D1}(Asp-99)–O^H(Tyr-73)	2.50	2.65	2.64	2.62	2.67
Environment of substrate					
O^{21}(SUB)[a]–CAL		2.41	2.22	2.40	2.24
O^{21}(SUB)–H^N(Gly-30)		2.27	1.91	2.09	2.00
C^{21}(SUB)–N^D(His-48)		4.45	3.29	4.44	3.32
C^{21}(SUB)–O(Wat-1)		3.20	—	3.01	—
O^{31}(SUB)–CAL		2.22	2.21	2.21	2.21
Hydrogen bonds of His–Asp					
N^D(His-48)–H^1(Wat-1)		1.92	—	2.01	—
H^{ND}(His-48)–O^H(SUB)		—	1.87	—	1.82
H^{ND}(His-48)–O^2/N^2(SUB)		—	1.84	—	1.98
H^{NE}(His-48)–O^{D2}(Asp-99)		1.71	1.60	1.69	1.61
O^{D2}(Asp-99)–H^{OH}(Tyr-52)		2.21	2.09	1.81	2.29
O^{D2}(Asp-99)–H(Wat-4)		1.79	1.81	1.91	1.83
O^{D1}(Asp-99)–H^{OH} (Tyr-73)		1.70	1.68	1.69	1.72
O^{D1}(Asp-99)–H(Wat-3)		1.72	1.74	1.70	1.77

Atom labels are described in Figure 5. [a] SUB refers to ester/amide as appropriate. [b] CAL refers to the calcium ion. Models B–E are the final models used for the MO calculations (*i.e.* after QM optimisation of QM atoms).

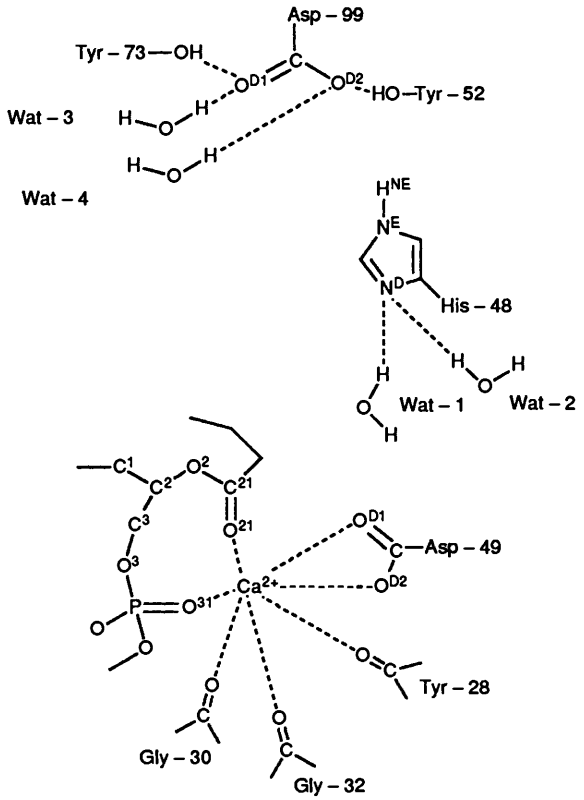

Figure 5. The essential features of the active site of PLA2, showing the residues which form the calcium binding loop and the residues hydrogen bonded to the His–Asp couple.

demonstrate that the geometry of the active site is highly preserved between the various MM models.

The ester and amide phospholipids bind in the same manner. The C^2 carbonyl and phosphate are bound tightly to the calcium ion, which may be of importance in ensuring correct alignment of the carbonyl to the attacking water and His-48. This water molecule (originally from the crystal co-ordinates) is found to be hydrogen-bonded to N^D of His-48, with the oxygen approximately 3 Å from the carbon atom of the carbonyl. The second hydrogen of this water is found to be hydrogen-bonded to the carboxylate of Asp-49 (one of the calcium ligands), which may limit the mobility of this water, although this hydrogen bond can break during molecular dynamics simulations.

The important features of the active site can be described briefly (Figure 5). The calcium ion is bound in a loop comprising of the carbonyls of Tyr-28, Gly-30, and Gly-32 and the carboxylate of Asp-49. His-48 is hydrogen-bonded to Asp-99 and a further water molecule (which moves away on protonation of N^D). Asp-99 hydrogen-bonds to two tyrosine hydroxy groups and to two water molecules, though some of these hydrogen bonds are more labile than others.

As previously described, the oxyanion was fitted into the active site by the constraint of the hydrogen bonds from H^{ND} of His-48 to O^2 and O^H of the oxyanion during the initial minimisation. This resulted in minor deformation of the oxyanion to produce the doubly hydrogen bonded structure (Figure 2), which may be expected to allow the facile proton transfer from water to His-48 and then to the substrate. In this structure, the hydroxy group of the oxyanion occupies the same position in space as the nucleophilic water. Thus the reaction can be seen as one which involves the movement of the substrate carbonyl towards a stationary water, and not the movement of water towards the carbonyl. Although the phospholipid oxyanions do not form the structure in Figure 2 readily during MM minimisation, we believe the structure to be valid because it is achieved on energy minimisation with small oxyanions in the active site, and also when molecular dynamics on the full-size substrates was performed. The amide oxyanion was found to take up the same position in the active site as the ester oxyanion, which suggests that the difference in the rates of hydrolysis of ester and amide is entirely due to the relative resistance to hydrolysis of the amide bond.

Table 2. ΔE_{QM} and $\Delta E_{MM/QM}$ (kcal mol^{-1}) for models I–III for ester and amide hydrolysis, using 4-31G basis: I, substrate + water + imidazole ⟶ intermediates, *in vacuo*; IIa, as I plus acetate, single proton transfer; IIb, as IIa but *in situ*; IIIa, as I plus acetate, double proton transfer; IIIb, as IIIa but *in situ*.

Model	ΔE_{QM}	$\Delta E_{MM/QM}$	ΔE_{Total}
Ester			
I	+36.4		
IIa	+19.1		
IIb	−8.0	+8.0	0.0
IIIa	+33.8		
IIIb	+20.2	+6.2	+26.4
Amide			
I	+54.4		
IIa	+37.0		
IIb	+22.9	+5.1	+28.0

QM–MM Calculations.—QM–MM Optimisations. The combination of QM and MM gradients during QM optimisation allows the investigation of the structure of a reactive intermediate *in situ*, in that steric and electronic interactions with the active site are allowed to influence the optimisation of the QM atoms. Figure 6 presents examples of the geometries of the substrates obtained by the QM–MM optimisation compared with those obtained for an optimisation *in vacuo*. Both sets of structures are very similar, with some distortions in dihedral angles such that the *in situ* structures tend to be several kcal mol^{-1} higher in energy. The oxyanions formed from the ester and amide phospholipids are again very similar.

Single versus *Double Proton Transfer Mechanisms.* Table 2 lists the enthalpies of hydrolysis, ΔE_{QM}, for the various models. For the models evaluated *in situ*, *i.e.* where point charges are included for all MM atoms, ΔE_{QM} comprises the electronic energy, the nuclear energy (the interaction of the QM nuclei) and a nuclear repulsion term (the interaction of the point charges with the QM nuclei). $\Delta E_{MM/QM}$ is the MM energy of interaction of the MM atoms with the QM atoms, without MM electrostatic terms.

For the ester phospholipid, the barrier to hydrolysis in the simplest *in vacuo* model (model I) is large (+36.4 kcal mol^{-1}), which is reduced on the addition of acetate by 17.3 kcal mol^{-1} for the single proton transfer model (IIa), but by only 2.6 kcal mol^{-1} for the double proton transfer model (IIIa). When the QM system is surrounded by the field of point charges, ΔE_{QM} for single proton transfer is reduced by 27.1 kcal mol^{-1} to 8.0 kcal mol^{-1} (model IIb), and for the double proton transfer is reduced by 13.6 kcal mol^{-1} to +22.9 kcal mol^{-1} (model IIIb). Overall then, the addition of acetate and the field of point charges has reduced ΔE_{QM} by a total of 44.4 kcal mol^{-1} for the single proton transfer, which is found to be more favourable than the double proton transfer by some 28 kcal mol^{-1}. This stresses the role of the ionic triad of oxyanion–imidazolium–acetate in the reduction of the barrier to hydrolysis, which

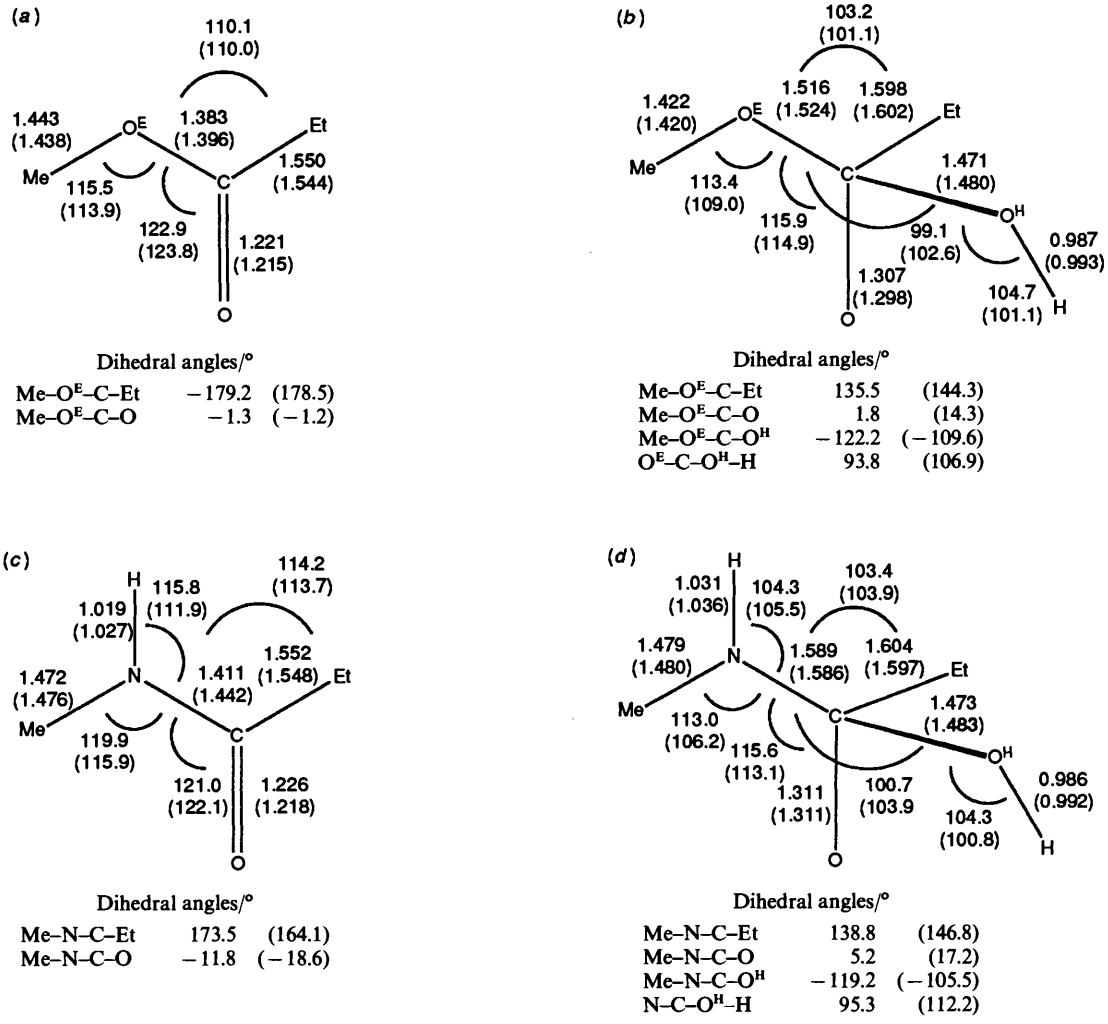

Figure 6. STO-3G optimised geometries for the ester, ester oxyanion, amide and amide oxyanion. Values without brackets are obtained *in situ* (*i.e.* with the combined QM–MM method), while, for comparison, values within brackets are obtained *in vacuo*. Lengths are quoted in Å, angles in °.

results from the electrostatic interactions both within the triad and between the triad and the environment. These stabilising electrostatic interactions are lost when the double proton transfer occurs, when the ionic imidazolium and acetate become neutral. Hence the role of aspartate is seen to be purely electrostatic, and it is not necessary to postulate any mechanism which involves the second proton transfer or substantial charge transfer between histidine and aspartate.[10,11,28]

$\Delta E_{MM/QM}$ for single proton transfer is +8.0 kcal mol^{-1} which shows that the active site tends to destabilise the formation of the oxyanion. This figure comprises the MM bond/angle/dihedral energies across the QM–MM junction (+4.9 kcal mol^{-1}, mostly due to dihedral distortion in the oxyanion) and non-bonded interactions between QM and MM atoms ($\Delta E_{\text{hydrogen bond}}$ +0.5 kcal mol^{-1}, $\Delta E_{\text{van der Waals}}$ +2.6 kcal mol^{-1}). The value of $E_{MM/QM}$ is also quite small (−23 kcal mol^{-1} for the reactants of IIb). The MM energy within the MM atoms was also evaluated, as a measure of the distortion in the enzyme required to fit the oxyanion. However, this gave rise to very large absolute electrostatic energies, such that $\Delta E_{\text{electrostatic}}$ is also very large, which in effect swamps the small value expected of ΔE_{MM}. Despite this, the non-electrostatic energies of ΔE_{MM} can be used to demonstrate that no significant distortion of the enzyme is present. Thus, ΔE_{MM} without electrostatic terms is small, in this case −6.6 kcal mol^{-1}.

Table 3. Mulliken atomic charges at the ester and amide groups for the QM models IIa and IIb. C and O refer to the carbonyl group, O^E is the ether oxygen of the ester.

Ester		O^E	C	O
IIa Substrate		−0.73	+0.81	−0.61
Oxyanion		−0.81	+0.82	−0.84
IIb Substrate		−0.71	+0.88	−0.80
Oxyanion		−0.81	+0.89	−1.09
Amide	**H**	**N**	**C**	**O**
IIa Substrate	+0.35	−0.85	+0.78	−0.65
Oxyanion	+0.29	−0.84	+0.74	−0.84
IIb Substrate	+0.37	−0.85	+0.84	−0.85
Oxyanion	+0.30	−0.85	+0.81	−1.09

Amide versus *Ester Hydrolysis.* For the amide phospholipid ΔE_{QM} in the initial model (I) is much larger than for the ester (+54.4 *versus* +36.4 kcal mol^{-1}). Addition of acetate reduces ΔE_{QM} by a similar amount (17.4 kcal mol^{-1}). However, the addition of the field of point charges (model IIb) reduces ΔE_{QM} by only 14.1 kcal mol^{-1} to +22.9 kcal mol^{-1}. Thus the active site stabilises the amide oxyanion less effectively than the ester oxyanion. The reason for this is suggested by the charge

Table 4. ΔE_{QM} (kcal mol^{-1}) for ester hydrolysis (single proton transfer, *in situ*, 4-31G basis). Model IVa is based on model IIb but with Asp-99 represented by point charges. Models b–f differ from IVa by the alteration of charges for the following functional groups: IVb, omits C^3 ethanolamine chain; IVc calcium becomes +1.8; IVd, calcium becomes +1.0; IVe, omits calcium and carbonyl ligands; IVf, as for IVe, omits C^3 phosphate and ethanolamine.

Model	ΔE_{QM}
IVa	−16.6
IVb	−15.5
IVc	−9.9
IVd	−15.8
IVe	+40.8
IVf	+32.9

distribution around the carbonyl (Table 3 presents 4-31G Mulliken populations). The electrostatic interaction between calcium and the oxyanion will be greater than that between calcium and the ester, simply because of the greater electron density on the oxyanion oxygen, which leads to the reduction in ΔE_{QM}. Comparison of the amide with the ester shows that the amide carbonyl is more polarised than the ester carbonyl, whereas both oxyanions are similarly polarised. The slight increase in electron density on the amide oxygen results in a smaller decrease in ΔE_{QM} than is seen for the ester. $\Delta\Delta E_{QM}$ between ester and amide is therefore large (31 kcal mol^{-1}), which is consistent with the experimental finding that the amide is not hydrolysed. $\Delta E_{MM/QM}$ for the amide is similar to that for the ester.

Interaction Energies within the Models. Calculation of the energies of individual molecules allows the evaluation of interaction energies within the supermolecule models. These are found to be very large, particularly between charged residues. Thus, the interaction energy between the lipid oxyanion and imidazolium (*in vacuo*, 4-31G) is −101 kcal mol^{-1}, compared with the ester–water–imidazole interaction energy of −7.6 kcal mol^{-1}. The binding of acetate to the oxyanion–imidazolium system releases 49.1 kcal mol^{-1} compared with 31.9 kcal mol^{-1} for binding to the ester–water–imidazole system.

These large stabilising interactions, mostly electrostatic in origin, are reduced *in situ* by the effective dielectric within the protein. In our models, the presence of the field of point charges provides, to a first approximation, a dielectric for the system. This can be demonstrated by comparing model IIb (ester hydrolysis in the full field of charges) with two modified models. Model IIc has the field of charges reduced to only the polar groups immediately surrounding the supermolecule (*i.e.* calcium, the carbonyls which are calcium ligands, the tyrosine hydroxy groups, and water molecules hydrogen-bonded to the His–Asp couple, the substrate phosphate and ethylammonium chain). Model IId has no charges except for the +2 of calcium. ΔE_{QM} for model IId is now very large (−46.9 kcal mol^{-1}), while model IIc (−26.9 kcal mol^{-1}) is intermediate between IId and the full field of charges, IIb (−8.0 kcal mol^{-1}). The field of charges dampens the large interaction between the supermolecule and the calcium (this interaction is calculated as −159 kcal mol^{-1} for the ester supermolecule, −225 kcal mol^{-1} for the oxyanion supermolecule). With model IIa as a baseline, the effect of a bare calcium charge is to reduce ΔE_{QM} by 66.0 kcal mol^{-1}. This is attenuated by the presence of the small field of charges (model IIc) to a reduction of 45.9 kcal mol^{-1}, and by the full field of charges (model IIb) to a reduction of 27.1 kcal mol^{-1}. Therefore, the full field of charges provides a screening of 66.0/27.1 (*ca.* 2.4), which compares with the dielectric of 2–3 often quoted for the protein interior,[40] although the dielectric is much higher at a protein–water interface. The smaller field of charges clearly does not provide a sufficient screening effect. The use of a field of charges is not an ideal approximation of the complex dielectric of the protein–solvent system as this model does not describe the polarisation within the protein. However, it is unlikely that a refined dielectric model would alter qualitatively our findings. Again, some of the approximations of the model are cancelled out when we use it to obtain relative energies between ester and amide hydrolysis.

Modifications to the Field of Charges. A series of single-point calculations were performed on the ester system to investigate the dependence of ΔE_{QM} on small perturbations to the field of point charges. To reduce the computation involved, in these models Asp-99 was also represented by point charges. This resulted in a lower ΔE_{QM} (−16.6 kcal mol^{-1}, Table 4, model IVa), although $\Delta E_{MM/QM}$ was higher (+10.6 kcal mol^{-1}). When the standard AMBER charges of Asp-99 were replaced with electrostatic potential charges (generated from a wavefunction polarised by the active site charges), a further lowering of ΔE_{QM} resulted. This highlights the problem of performing MO calculations in a field of charges, *i.e.* that the wavefunction is extremely sensitive to the value of the charges. Thus valid comparisons of E_{QM} can only be made between systems where the fields of charges have been generated in an identical manner, such as with the same distance cut-off, or the same all-atom or united-atom representation of residues. In this case, the problem is probably one of choice of residues which need to be treated explicitly and which can be represented by point charges. The discrepancy noted for model IVa may arise because a small degree of charge transfer occurs between Asp-99 and His-48 (as determined by Mulliken population analysis), and therefore a point charge model can never adequately reproduce the Asp–His interaction. However, for the purposes of models IVa–IVf the charge representation of Asp-99 is used, and hence ΔE_{QM} for these models should only be compared against the base-line value of model IVa.

In model IVb the point charges representing the C^3 ethanolamine chain are omitted. Only a small change in ΔE_{QM} is observed (+1.1 kcal mol^{-1}) which indicates that the presence of the +1 charge of the ammonium group has little effect on the hydrolysis of the substrate. This is consistent with the observation that PLA2 can hydrolyse phospholipids in which ethanolamine is replaced by a variety of small molecules (including neutral residues).[1]

The other models demonstrate the sensitivity of ΔE_{QM} to the presence of calcium. PLA2 has a strict requirement for Ca^{2+}, in that in the presence of other ions substrate binding occurs but there is no hydrolysis.[1] The only ion which can replace Ca^{2+} with some retention of activity is Gd^{3+}, which is of a similar size. (Recently it has been demonstrated that Lys-49–PLA2 probably has no activity:[41] here the ammonium side-chain of Lys-49 replaces Ca^{2+} in substrate binding).

Model IVc has the charge which represents calcium reduced to +1.8, crudely simulating the smaller effective charge experienced by the substrate in the presence of a larger divalent cation. ΔE_{QM} is then increased by 6.7 kcal mol^{-1}, while if the charge is reduced to +1 (model IVd), ΔE_{QM} is increased by 32.4 kcal mol^{-1}. If the charges of calcium and its carbonyl ligands are removed altogether (model IVe), ΔE_{QM} is 57.4 kcal mol^{-1} higher than model IVa, whilst if in addition the charges of the phosphate and the remainder of the C^3 chain are also removed (model IVf), the difference is 49.5 kcal mol^{-1}. Hence this simple model demonstrates that ΔE_{QM} is very sensitive to the magnitude of the charge on the calcium. Although part of the action of calcium is to neutralise the negative charge of the phosphate (which lies very close to the C^2 carbonyl), the major role is likely to be to polarise the substrate and/or stabilise the oxyanion. Although the backbone NH of Gly-30 is at hydrogen-bonding distance from the carbonyl oxygen, it would be unlikely to

Table 5. Comparison of ΔE_{QM} (kcal mol^{-1}) for different basis sets.

	ΔE_{QM}			
	STO-3G	4-31G	6-31G**	6-31G**/MP2
Model V[a]	−94.4	−29.7	−39.0	−35.4
Model VIa[b]				
Formic acid	+85.7	+38.2	+57.8	+48.9
Formamide	+81.6	+54.8	+65.9	+53.1
Model VIb[c]				
Formic acid	+60.6	+21.2	+39.3	+30.4
Formamide	+62.0	+44.3	+53.1	+40.1

[a] Model V: $NH_4^+ + HCOO^- \longrightarrow NH_3 + HCOOH$. [b] Model VIa: formic acid, $HCOOH + HOH + NH_3 \longrightarrow HCOOH{\cdot}OH^- + NH_4^+$; formamide, $HCONH_2 + HOH + NH_3 \longrightarrow HCONH_2{\cdot}OH^- + NH_4^+$. [c] Model VIb, as for VIa but with addition of +1 point charge.

Table 6. Absolute energies of reactants for selected QM models (by use of a 4-31G basis unless otherwise stated). For *in situ* calculations, E_{QM} includes charge–nuclei interactions but not charge–charge interactions.

Reactant	Model	Basis set	E_{QM}/a.u.
Ester	I		−605.788 871
	IIa		−832.724 226
	IIb		−833.122 741
	IIc		−832.920 563
	IId		−832.978 187
	IVa		−605.916 617
	IVb		−605.910 207
	IVc		−605.901 726
	IVd		−605.851 950
	IVe		−605.823 359
	IVf		−605.824 916
	V	STO-3G	−241.531 983
		4-31G	−244.533 668
		6-31G**	−244.899 930
		MP2[a]	−0.710 707
Amide	I		−585.987 954
	IIa		−812.923 335
	IIb		−813.336 058
Formic acid	VIa	STO-3G	−316.649 150
		4-31G	−320.488 708
		6-31G**	−320.985 901
		MP2	0.905 055
	VIb	STO-3G	−316.674 820
		4-31G	−320.529 735
		6-31G**	−321.023 197
		MP2	−0.900 926
Formamide	VIa	STO-3G	−297.116 909
		4-31G	−300.690 622
		6-31G**	−301.154 331
		MP2	−0.894 272
	VIb	STO-3G	−297.150 882
		4-31G	−300.743 839
		6-31G**	−301.202 200
		MP2	−0.889 681

[a] MP2 is the calculated correlation energy.

contribute much to the stability of the substrate/oxyanion when compared with the magnitude of the electrostatic interaction with calcium. However, the hydrogen-bond may have a role in the positioning of the carbonyl *in situ*. The results from the preceding sections present evidence in favour of the binding of the substrate carbonyl at the calcium (as opposed to at any other site in the active site), in that they highlight the essential role of calcium and present a possible reason for the ester *versus* amide specificity.

Table 7. Partial charges calculated by the electrostatic potential method for ester and amide group used in the free energy perturbation calculations. *in vacuo* charges were used for the desolvation calculation, *in situ* charges for binding calculation. O^E is the ether oxygen.

in vacuo charges				*in situ* charges			
Ester		Amide		Ester		Amide	
		H	+0.266			H	+0.280
O^E	−0.373	N	−0.550	O^E	−0.373	N	−0.551
C	+0.838	C	+0.746	C	+0.915	C	+0.822
O	−0.444	O	−0.430	O	−0.573	O	−0.561

Large Basis Set Calculations. A series of calculations were performed with larger basis sets in order to investigate the basis set dependency of the preceding calculations. A number of simplified models were considered. The proton transfer between ammonium and formate (model V, Figure 4) was taken as a model for proton transfer between His-48 and Asp-99, and the attack of water on formic acid and formamide, with proton transfer to ammonia (model VI) was taken to represent ester *versus* amide hydrolysis. The latter model was repeated in the presence of a single +1 point charge to represent the calcium ion. For each supermolecule model, *in vacuo* STO-3G geometries were used for each monomer, with intermolecular geometries approximating those found in PLA2. ΔE_{QM} was evaluated by single-point calculations using the following basis sets: STO-3G; 4-31G; 6-31G**; 6-31G**/MP2.

The results for the ammonium–formate system (Table 5) highlight the discrepancy between STO-3G and the higher basis sets, the results for the latter being of comparable energy. A similar pattern is found for the formic acid *versus* formamide results. Inclusion of the MP2 perturbation energy as an estimation of electron correlation effects, to some extent reverses the effect of adding d and p polarisation functions (6-31G**). The 4-31G energies appear to be within about 10 kcal mol^{-1} of 6-31G**/MP2 energies.

Comparison of the 4-31G and 6-31G**/MP2 results (when the latter are taken as the 'best' achievable) indicates that the 4-31G basis set cannot be taken as strictly quantitative, but does reproduce the essential features of substrate specificity. Formic acid is shown to be more readily hydolysed than formamide, although the difference is overestimated at the 4-31G level. The effect of addition of a point charge is to reduce ΔE_{QM} for both substrates, with amide hydrolysis being stabilised to a lesser extent. The 4-31G basis is better at reproducing formamide energies than those of formic acid, and also reproduces well the stabilisation wrought by the point charge. In conclusion, 4-31G is clearly not ideal, but then neither is 6-31G** without the inclusion of correlation energies. In the simulation of enzyme catalysis, a compromise must be made between the choice of large basis sets and large QM systems and with present computational resources 4-31G may be seen as a satisfactory compromise.

The 6-31G**/MP2 results again demonstrate the substrate specificity of the system. Formamide binds more strongly to the point charge than does formic acid (−27.1 *versus* −20.8 kcal mol^{-1}) while both oxyanions bind similarly (−40.1 *versus* −39.3 kcal mol^{-1} for amide and acid, respectively). Hence the point charge will stabilise formic acid hydrolysis to a greater extent than amide hydrolysis.

Table 6 presents absolute values of E_{QM} for the above models.

Free-energy Perturbation Calculations.—We have carried out the free-energy perturbation calculations for the mutation of the small amide into ester in a box of water, and for the mutation of the amide phospholipid into the ester phospholipid in the active site, by use of the point charges given in Table 7. ΔG for desolvation (amide ⟶ ester) was found to be $+0.62 \pm 0.11$ kcal mol^{-1}, which shows that the amide is more strongly solvated. ΔG of binding (amide ⟶ ester) was determined by the window method to be $+4.22 \pm 0.18$ kcal mol^{-1} and by the slow growth method to be $+4.33 \pm 0.25$ kcal mol^{-1}, which gives an overall value of $+4.28 \pm 0.21$ kcal mol^{-1}. Therefore the amide binds more strongly by some 3.7 kcal mol^{-1}, if one takes into account desolvation of the substrate. Thus the results are in qualitative agreement with the QM results that the amide binds more strongly than the ester and agree quantitatively with the experimental data[38] which suggest a difference in rates of binding of approximately a factor of 10, which infers a value of $\Delta G_{binding}$ of *ca.* 2 kcal mol^{-1}.

Conclusions

We have presented calculations on the energetics of phospholipid hydrolysis in the active site of PLA2. A relatively simple computational model can explain, to some degree, the catalytic role of the active site, and is able to quantify differences in binding and hydrolysis between a substrate and an inhibitor. Although only one mechanism of catalysis has been investigated, it is clear that this mechanism is in accord with the limited experimental data, and has been shown in this paper to be feasible in that the active site is capable of reducing the large barrier to hydrolysis.

Similar modes of binding have been found for ester and amide phospholipids. Interaction of the C^2 carbonyl with the calcium appears to be necessary to reduce the barrier to hydrolysis, which may account for the known specificity for calcium, and provide a mechanism for ester *versus* amide specificity. On energetic grounds, we suggest that an oxyanion doubly hydrogen bonded to His-48 may be a realistic intermediate, whereas a double proton transfer mechanism involving Asp-99 is unfavourable.

The approximations inherent in our method limit its usefulness to obtain absolute energies of binding or hydrolysis, but it is valuable in the exploration of the relative rates of reaction between similar substrates. Although all computational methods must rely on experimental verification, the great value of such methods is in the elucidation and prediction of mechanistic detail which may otherwise be elusive.

Acknowledgements

We thank the SERC for support of this research under grant GR/E53682 and GR/F49934.

References

1 A. J. Slotboom, H. M. Verheij, and G. H. de Haas, *New Comprehensive Biochemistry*, 1982, **4**, 354.
2 H. M. Verheij, J. J. Volwerk, E. H. Jansen, W. C. Puyk, B. W. Dijkstra, J. Drenth, and G. H. de Haas, *Biochem.*, 1980, **19**, 743.
3 B. Waszkowycz, I. H. Hillier, N. Gensmantel, and D. W. Payling, *J. Chem. Soc., Perkin Trans. 2*, 1989, 1795.
4 J. M. Blaney, P. K. Weiner, A. Dearing, P. A. Kollman, E. C. Jorgensen, S. Oatley, J. Burridge, and C. C. F. Blake, *J. Am. Chem. Soc.*, 1982, **104**, 6424.
5 G. Wipff, A. Dearing, P. K. Weiner, J. M. Blaney, and P. A. Kollman, *J. Am. Chem. Soc.*, 1983, **105**, 997.
6 D. M. Hayes and P. A. Kollman, *J. Am. Chem. Soc.*, 1976, **98**, 7811.
7 L. C. Allen, *Ann. N.Y. Acad. Sci.*, 1981, **367**, 383.
8 S. Nakagawa and H. Umeyama, *J. Theor. Biol.*, 1982, **96**, 473.
9 J. A. C. Rullmann, M. N. Bellido, and P. T. van Duijnen, *J. Mol. Biol.*, 1989, **206**, 101.
10 S. Nakagawa and H. Umeyama, *J. Mol. Biol.*, 1984, **179**, 103.
11 H. Umeyama, S. Hirono, and S. Nakagawa, *Proc. Natl. Acad. Sci. USA*, 1984, **81**, 6266.
12 G. Bolis, M. Ragazzi, D. Salvaderi, D. R. Ferro, and E. Clementi, *Gazz. Chim. Ital.*, 1978, **108**, 425.
13 G. Alagona, P. Desmeules, C. Ghio, and P. A. Kollman, *J. Am. Chem. Soc.*, 1984, **106**, 3623.
14 S. J. Weiner, G. L. Seibel, and P. A. Kollman, *Proc. Natl. Acad. Sci. USA*, 1986, **83**, 649.
15 A. Warshel and M. Levitt, *J. Mol. Biol.*, 1976, **103**, 227.
16 U. C. Singh and P. A. Kollman, *J. Comput. Chem.*, 1986, **7**, 718.
17 P. K. Weiner and P. A. Kollman, *J. Comput. Chem.*, 1981, **2**, 287.
18 M. F. Guest and J. Kendrick, GAMESS User Manual, CCP1/86/1, Daresbury Laboratory, UK, 1986.
19 B. L. Tembe and J. A. McCammon, *Comp. Chem.*, 1984, **8**, 281.
20 W. J. Jorgensen and C. Ravimohan, *J. Chem. Phys.*, 1985, **83**, 3050.
21 U. C. Singh, F. K. Brown, P. A. Bash, and P. A. Kollman, *J. Am. Chem. Soc.*, 1987, **109**, 1607.
22 C. F. Wong and J. A. McCammon, *J. Am. Chem. Soc.*, 1986, **108**, 3830.
23 P. A. Bash, U. C. Singh, F. K. Brown, R. Langridge, and P. A. Kollman, *Science*, 1987, **235**, 574.
24 K. M. Merz and P. A. Kollman, *J. Am. Chem. Soc.*, 1989, **111**, 5649.
25 S. R. Rao, U. C. Singh, P. A. Bash, and P. A. Kollman, *Nature*, 1987, **328**, 551.
26 V. Daggett, F. Brown, and P. A. Kollman, *J. Am. Chem. Soc.*, 1989, **111**, 8247.
27 D. M. Blow, J. J. Birktoft, and B. S. Hartley, *Nature* (*London*), 1969, **221**, 337.
28 A. A. Kossiakoff and S. A. Spencer, *Biochem.*, 1981, **20**, 6462.
29 T. A. Steitz and R. G. Shulman, *Ann. Rev. Biophys. Bioeng.*, 1982, **11**, 419.
30 P. A. Kollman and D. M. Hayes, *J. Am. Chem. Soc.*, 1981, **103**, 2955.
31 B. W. Dijkstra, K. H. Kalk, W. G. J. Hol, and J. Drenth, *J. Mol. Biol.*, 1981, **147**, 97.
32 S. J. Weiner, P. A. Kollman, D. A. Case, U. C. Singh, C. Ghio, G. Alagona, S. Profeta, and P. Weiner, *J. Am. Chem. Soc.*, 1984, **106**, 765.
33 S. J. Weiner, P. A. Kollman, D. T. Nguyen, and D. A. Case, *J. Comput. Chem.*, 1986, **7**, 230.
34 U. C. Singh and P. A. Kollman, *J. Comput. Chem.*, 1984, **5**, 129.
35 P. B. Hitchcock, R. Mason, K. M. Thomas, and G. G. Shipley, *Proc. Natl. Acad. Sci. USA*, 1974, **71**, 3036.
36 CADPAC. The Cambridge Analytic Derivatives Packages, Issue 4.0, R. D. Amos and J. E. Rice, Cambridge, 1987.
37 P. P. M. Bonsen, G. H. de Haas, W. A. Pieterson, and L. L. M. van Deenen, *Biochim. Biophys. Acta*, 1972, **270**, 364.
38 G. H. de Haas, M. G. van Oort, R. Dijkman, and R. Verger, *Biochem. Soc. Trans.*, 1989, **17**, 274.
39 M. M. Campbell, J. Long-Fox, D. J. Osguthorpe, M. Sainsbury, and R. B. Sessions, *J. Chem. Soc., Chem. Commun.*, 1988, 1560.
40 M. K. Gilson and B. H. Honig, *Nature*, 1987, **330**, 84.
41 C. J. Van den Bergh, A. J. Slotboom, H. B. Verheij, and G. H. de Haas, *J. Cell. Biol.*, 1989, **39**, 379.

Paper 0/00331J
Received 22nd *January* 1990
Accepted 13th *March* 1990